Wind Integrated UPFC System with Cascaded Fuzzy Logic Controller for Alleviation of PQ Issues

Vinay Kumar Polishetty[1,*], G. Balamurugan[1], and Kartigeyan Jayaraman[1]

ARTICLE INFO

Article history:
Received: 20 May 2023
Revised: 24 June 2023
Accepted: 16 January 2024
Online: 20 June 2024

Keywords:
Power Quality
DFIG-WECS
IHHO-PI
UPFC
CFLC

ABSTRACT

A great deal of attention has been paid for improving Fault Ride-Through (FRT) capability of entire electric power system as a result of rising number of Doubly Fed Induction Generator-based Wind Energy Conversion Systems (DFIG-WECS) installed around the world. Due to variation in operating conditions at load side, the performance of DFIG is highly sensitive to variations as well as disturbance events. However, it is quite common for electrical systems to encounter problems caused by unstable nature and power quality owing to large number of nonlinear load charges in the system. It is therefore essential to limit the inner difficulties and bring about fine voltage quality distresses within the load. The aim of this research is to develop a Unified Power Flow Controller (UPFC), that improve overall dynamic performance of DFIG-WECS under wind gusts as well as enhances the FRT capability of DFIG in case of various disruption events occurring. The proposed series and shunt converters is controlled by implementing a Cascaded Fuzzy Logic Controller (CFLC) in order to evaluate their effectiveness. Moreover, to strengthen the DC voltage of DFIG-WECS, Improved Harris Hawks Optimized Proportional Integral (IHHO-PI) controller is introduced. Henceforth, the proposed work contributes in providing harmonics free supply to the load. The proposed framework is validated using MATLAB with two criteria. The outcomes reveals that, system established offers good response towards Power Quality (PQ) issues with improved THD value of 2.12%, which is comparatively low than state-of-art techniques.

1. INTRODUCTION

The progress of economy and society depends heavily on energy. As fossil fuels run out and threat of temperature change grows, resources and ecosystem are becoming more of a barrier to energy production. Green economy, energy ecological conservation, and sustainable energy production are the three main goals towards which the world is currently focusing. Power usage is steadily rising as a result of population increase and urbanization. The only way to stop this calamity is to worldwide develop sustainable energy worldwide [1, 2].

Advancements in DG technologies, comprising fuel cells, wind turbines, photovoltaics (PV) [3], and the invention of new power electronics have caused increasing electricity requirement, a restructuring of utilities, an ecological policy, the increasing price of fuel, exhaustion of fossil fuels, and a growing demand for superior PQ and dependability from consumers are causing power industry to utilize these as alternative energy source to central power plant [4]. In this way, DG is able to fulfill customer's requirements in both stand-alone and grid-tied mode, depending on circumstances, and surplus power production is fed into load, increasing the consistency of power supply as a result. In spite of this, wind [5] and PV power generation are unreliable and suffer from poor performance quality due to undesirable environmental characteristics of dissimilarities in wind speed and solar radiation. In the future, smart grids will rely heavily on wind energy as most promising renewable sources of energy. Throughout past two decades, WECS have been increasingly integrated into existing electricity loads. 2018 saw a global growth of 600 GW from wind power, or 6% of global electricity consumption [6]. The superiority and dependability of power supply is improved by integrating these sources with mainstream power generation sources [7, 8].

As modern power networks develop, there is an increasing demand for power by virtue of finite resources. A variation in load demand and integration of renewable energy [9] with the grid power flow do not remain constant,

[1]*Department of Electrical and Electronics Engineering, Annamalai University, Chidambaram, India*.
**Corresponding author:* Vinay Kumar Polishetty; Email: vinaykumarpolishettyy@gmail.com.

which negatively affects power network stability. To meet the rising need for electrical energy, the construction of new lines of the transmission network has also been restrained due to commercial and substantial restrictions. In consequence, the supply services are forced to utilize actual assets in an excellent manner, resulting in overloaded transmission networks, low stability and looped power flows. To advance the performance of power network, network planners looked for new techniques [10, 11]. However, for the effective implementation and operation of variable renewable energy production, ancillary services like reactive power assistance and voltage stability mechanisms are necessary to establish technical viability and commercial feasibility [12].

To increase the reliability of electricity systems and power quality, FACTS devices are frequently used. FACTS devices come in a variety of forms, each having unique capabilities, benefits, and drawbacks. To offer control of transmission parameters that are important for load's effective functioning, FACTS device is utilized either alone or in conjunction with some other FACTS device [13, 14]. Numerous FACTS devices are used to improve load voltage profile and power quality, including the Static VAR Compensator (SVC), Static Synchronous Series Compensator (SSSC), Thyristor-Controlled Series Capacitor (TCSC), Static Synchronous Compensator (STATCOM) and D-STATCOM [15, 16]. The aforesaid approaches show advantages of reactive power control, improvement of voltage stability, increased transient stability and power factor corrections. However, limited ability to handle rapid voltage fluctuations, increased complexity and challenges during dynamic circumstances makes those system fail. Hence forth in the proposed work, UPFC [17] is established for solving PQ issues, which comprises of series and shunt converters in its configuration enabling system stability.

The traditional PI controllers are still in use today in a wide variety of applications relating to the electrical producing industry. This is because they are simple and easy to use. In order to link WECS with load, PI controllers were employed. However, even with all these characteristics, PI controllers cannot perform their assigned function if their hyperparameters are not properly determined. This paved the path for development of contemporary optimization techniques [18]. Many applications for optimization in electrical systems have been presented, in recent times. Heuristic methods are optimization techniques that allow to quickly derive an approximation of value of ideal solution. The objective is to resolve a number of issues in various contexts without altering the fundamentals of algorithm. WECS uses existent metaheuristic algorithms such the Artificial Neural Network [19], Whale Optimization Algorithm (WOA) [20], and Grey Wolf Optimization (GWO) [21] to achieve system stability. However, the aforesaid approaches fail to stabilize voltage and require more time [22]. Hence the proposed work utilizes an advanced bio-inspired algorithm termed IHHO-PI controller, owing to its behavior towards high voltage profile and time consuming characteristics.

Similarly, effective controlling of UPFC is required, approaches like Particle Swarm Optimization (PSO) and Genetic Algorithm (GA) are widely utilized [23]. PSO, however, has more favorable performances than GA. PSO seems to require less generations than GA to reach its final parameter values. PSO offers a more well-balanced mechanism and greater adaptation to capacities for both local and global investigation. Also, it is utilized to address a diversity of optimization issues in electrical power system, including issues with improving stability of system and placing capacitors [24]. Likewise, Fuzzy logic controller (FLC), is introduced to improve power quality of UPFC [25-27]. However, it is does not has the ability to handle non-liner operations with greater accuracy. As a result, this work presents CFLC, which has the ability to control both reactive and active power flow, regulate line voltage, and improve transient stability due to its superior performance towards non-linearities.

In the proposed work, WECS based UPFC is established for solving problems associated with power disturbances. For stabilizing the voltage generated from WECS, IHHO-PI controller is accomplished, while the reference signal generated by UPFC is controlled by dq theory based CFLC. Utilizing MATLAB Simulink, the proposed system's performance is evaluated.

2. PROPOSED SYSTEM

Power quality issues are the most serious difficulties a power system faces because of their variety and frequent occurrence. In the meantime, the growth of renewable energy has increased the need for an integrated system which combines the advantages of improving power quality and producing sustainable energy. Accordingly, an integrated WECS-UPFC and its control approach are discussed in this work, as seen in Fig. 1.

This research proposes a UPFC topology, which offers a flicker system with a steady voltage output, to overcome PQ concerns. Moreover, it stops network voltage fluctuations from impacting the voltage at load. For the controller circuit, CFLC is utilized to provide the best possible outcomes together with PWM generator with dq theory; the dq theory is used to analyze and control the electrical quantities in a synchronous rotating reference frame. Moreover, it simplifies the representation of three-phase electrical variables into two orthogonal components: d (direct) and q (quadrature). This facilitates precise control of actual and complex power flow, voltage regulation, and PQ improvement in the system. The PWM rectifier uses the IHHO, a recently discovered metaheuristic optimizer, to modify the output of DFIG-based WECS.

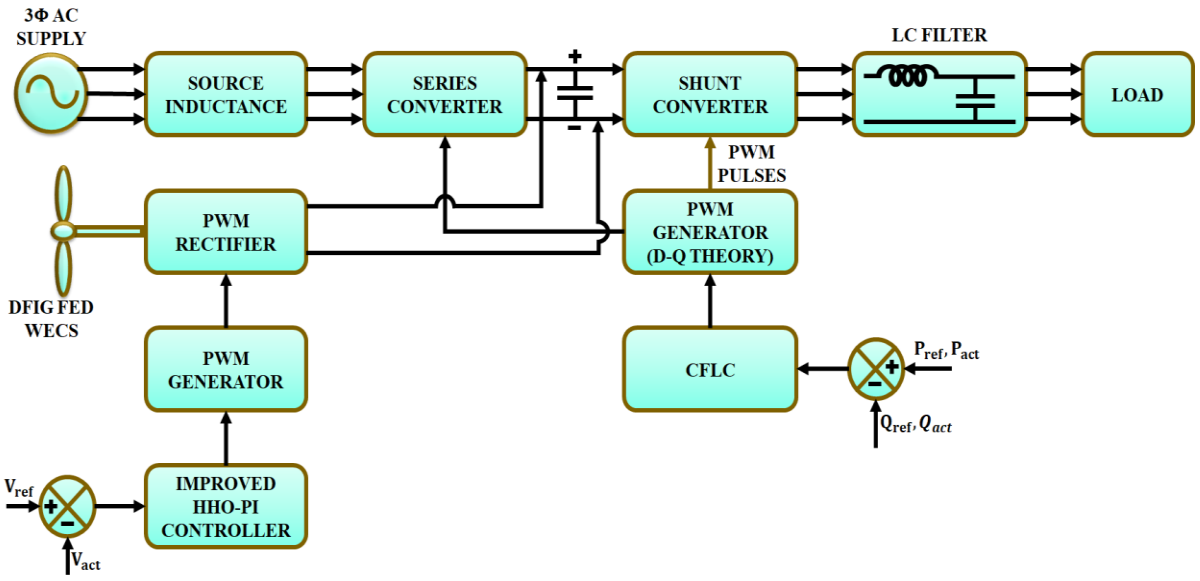

Fig. 1. Proposed Block Diagram.

The topology of suggested WECS-UPFC system comprises of four portions namely, WECS, series converter, shunt converter and DC bus. The series compensator is intended to address voltage quality issues like voltage sags and swells, whereas the parallel connection of shunt compensator at load side is employed to address current power quality issues like reducing the load's major reactive and harmonic power degradation. To carry out the WECS's purpose, the shunt converter is also meant to draw active electricity from wind system. A dc-bus is connected to series and shunt compensators, and the DC-link capacitor serves as a power energy buffer. The effectiveness of proposed work is examined utilizing MATLAB software and by displaying load voltage waveforms in instances of voltage sag, swell, transient, harmonics, and flickering for UPFC systems, the usefulness of UPFC is demonstrated.

2.1. Modelling Of UPFC

In recognition of its numerous benefits over other FACTS devices, UPFC is employed among a variety of FACTS devices. It is comprised of SSSC and STATCOM. A DC link is used to connect these two converters one after the other. All the variables, including phase angle, voltage and impedance, that have an impact on transmission of power is controlled concurrently or individually. After injection of voltage by UPFC in transmission line, it autonomously regulates the flow of actual and complex power thru line. The UPFC improves power systems' transient stability and voltage regulation. UPFC effectively regulates damping to prevent oscillations in power system.

2.1.1. Operating Principle of UPFC

Two voltage source converters (VSC) were used in UPFC arrangement depicted in Fig. 1. While the other is a series converter connected by a series transformer, the first is a shunt converter connected by a shunt transformer. A widespread DC link capacitor couples the converters back to back. This configuration unifies three main circuit functions of series, shunt and phase angle regulation. The primary job of a shunt converter, like a shunt compensator, is to provide or absorb active power from line. A DC link capacitor is charged by shunt converter, which also uses it to power series converter. To make up for any losses and real power generated or consumed by the series branch, a shunt branch is therefore required. V_{dc} cannot maintain an identical voltage if balance of power is not ensured.

By including a series voltage with the correct phase relationship, series converters provide both series and phase angle control. Reactive power cannot have a closed circuit between two converters connected by a DC link capacitor, whereas active power can have a closed channel through the converter. Voltage at series converter is specified as $V_{se}\angle\sigma$, in which controllable magnitude of voltage V_{se} is $V_{se}(0 \leq V_{se} \leq V_{semax})$ and $\sigma(0° \leq \sigma \leq 360°)$ is the phase angle with respect to voltage at sending end and is send to the series transformer. Line current is used to access this voltage source, which results in the transfer of both reactive and real power in line. Real power transferred at the AC terminal is converted by the inverter into DC power, which appears at the DC connection as required real power. Reactive power produced internally by the inverter gets transmitted at the AC terminal.

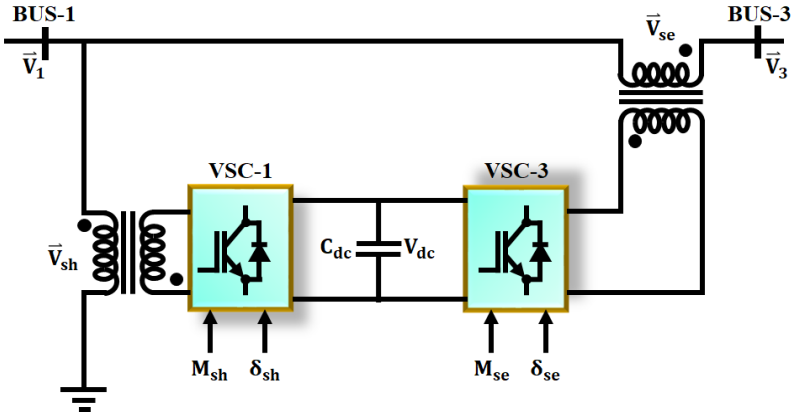

Fig. 2. UPFC configuration.

2.1.2. Source Modelling

The bus 1 is coupled to a 3Φ source. Once the current and voltage components have been translated to d-q frame of references,

$$v_d = v_{rms} cos\omega t \quad (1)$$

$$v_q = -v_{rms} sin\omega t \quad (2)$$

$$[C] = \begin{bmatrix} cos\theta & sin\theta \\ -sin\theta & cos\theta \end{bmatrix} \quad (3)$$

The reactive power component is expressed as

$$Q = -v_q i_d + v_d i_q \quad (4)$$

The component at real power is

$$p = v_d i_d + v_q i_q \quad (5)$$

The V-I relation of balanced 3Φ system is,

$$v_{ryb} = Z_{ryb} \times i_{ryb} \quad (6)$$

Let i_{ryb} be column vector of current that flows through Z_{ryb} impedance column matrix and v_{ryb} is specified as column vector of voltage sag across series connected of reactance and resistance in all 3 phases.

$$\begin{bmatrix} ea' - va' \\ eb' - vb' \\ ec' - vc' \end{bmatrix} = \begin{bmatrix} R + pL & 0 & 0 \\ 0 & R + pL & 0 \\ 0 & 0 & R + pL \end{bmatrix} \begin{bmatrix} ia \\ ib \\ ic \end{bmatrix} \quad (7)$$

The first column matrix in Expression (7) represents matrix of voltage drops on each side of impedances throughout all 3 phases.

On transformation to $\alpha\beta$ component the equation becomes

$$Z_{\alpha\beta} = \begin{bmatrix} R + pL & 0 \\ 0 & R + pL \end{bmatrix} \quad (8)$$

Change now into reference frame that rotates synchronously

$$Z_{dq} = \begin{bmatrix} R + pL & -\omega L \\ \omega L & R + pL \end{bmatrix} \quad (9)$$

After transformation, the expression for voltage is given by

$$\begin{bmatrix} ed' - vd' \\ eq' - vq' \end{bmatrix} = \begin{bmatrix} R + pL & -\omega L \\ \omega L & R + pL \end{bmatrix} \begin{bmatrix} id \\ iq \end{bmatrix} \quad (10)$$

where, synchronously rotating frequency is denoted as ω.

2.2. Design of Shunt Converter

The representation of shunt converter is shown in Fig. 3. In most cases, shunt inverters run in automatic voltage control mode. Shunt inverter reactivity current, which has preset drooping characteristics, maintains the transmission voltage constant at the point of link in voltage control mode. The actual voltage is measured on shunt transformer's receiving end bus. The regulated quantity in control strategy is the current i_{sh} that shunt converter draws.

$$v_{dsh} = v_{1d} + i_{dsh} r_{sh} + L_{sh} \frac{di_{dsh}}{dt} - \omega L_{sh} i_{qsh} \quad (11)$$

$$v_{qsh} = v_{1q} + i_{qsh} r_{sh} + L_{sh} \frac{di_{qsh}}{dt} + \omega L_{sh} i_{dsh} \quad (12)$$

Transform the equations into unit form.

$$v_{dsh} = v_{1d} + i_{dsh} r_{sh} + \frac{x_{sh}}{\omega} \frac{di_{dsh}}{dt} - x_{sh} i_{qsh} \quad (13)$$

$$v_{qsh} = v_{1q} + i_{qsh} r_{sh} + \frac{x_{sh}}{\omega} \frac{di_{qsh}}{dt} + x_{sh} i_{dsh} \quad (14)$$

$$v_{shrms} = \sqrt{v_{shd}^2 + v_{shq}^2} \quad (15)$$

$$P_{sh} = v_{dsh} i_{dsh} + v_{qsh} i_{qsh} \quad (16)$$

The controller that controls AC bus voltage provides shunt current i_{shq}^* for reactive power bearing portion, while the controller that controls the DC bus voltage provides reference for actual power bearing current i_{shp}^*. For sending end voltage, a PI control scheme is built assuming that the shunt converter is off. Main function of a shunt voltage calculator is to measure and calculate the required voltage for controlling the shunt converter. It ensures proper voltage regulation and stabilization in power system, facilitating effective control of complex power flow and voltage profile enhancement.

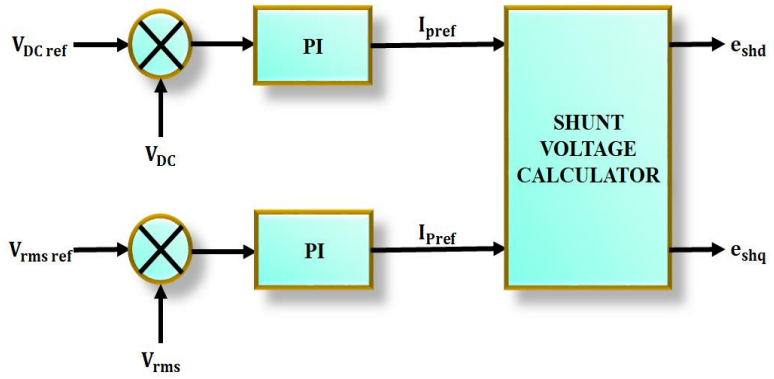

Fig. 3. Block Representation of Shunt Converter.

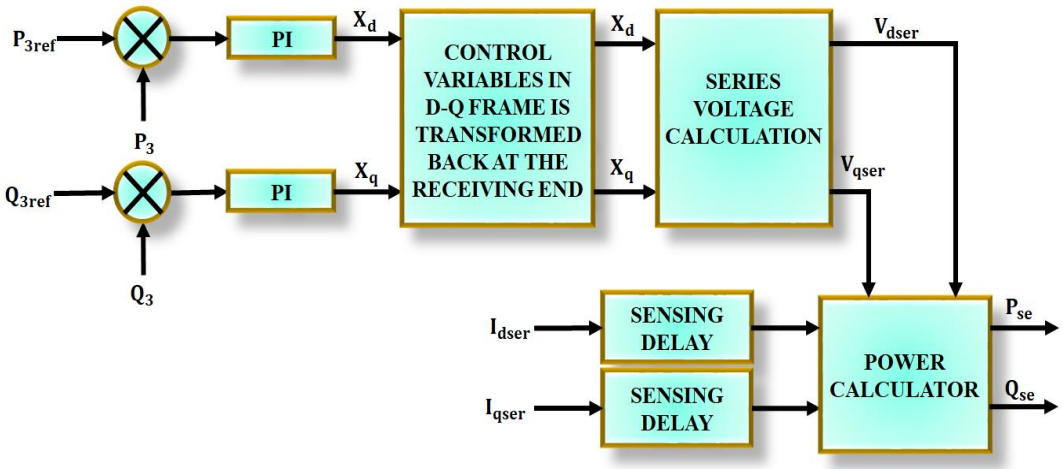

Fig. 4. Series Converter Block Diagram.

2.3. Design of Series Converter

Typically, a series inverter runs in automated power flow manner. This mechanism uses a synchronous reference frame, where control values are represented as dc quantities, to control the transmission line current. The PI controller, which has inputs P_{ref} and Q_{ref}, determined real and reactive power amounts, configure the relative real and reactive components.

The power system dynamics and shunt converter are not taken into consideration while designing series converters. The schematic diagram o series controller is displayed in Fig. 4. The sensing delay block in the presented series converter is used to introduce a controlled delay in the sensing of system parameters. This delay allows for accurate measurement and analysis of the system dynamics, enabling proper time alignment for control actions. By incorporating the sensing delay block, the series converter effectively responds to changes in the system and provide appropriate control signals, enhancing stability and performance.

Expressions of voltage and current decoupled is expressed as

$$v_{1d} + v_{dser} = v_{2d} \tag{17}$$

$$v_{1q} + v_{qser} = v_{2q} \tag{18}$$

$$v_{3d} = v_{2d} - i_{dse}r_{se} - \frac{x_{sh}}{\omega}\frac{di_{dse}}{dt} + x_{sh}i_{qse} \tag{19}$$

$$v_{3q} = v_{2q} - i_{qse}r_{se} - \frac{x_{sh}}{\omega}\frac{di_{qse}}{dt} + x_{sh}i_{dse} \tag{20}$$

The power at bus 3 is evaluated using values of $v_{2d}, v_{2q}, i_{dse}, i_{qse}$.

2.4. Dynamic Equation of DC Link Capacitance

Power balance theory is used to design DC link capacitance on the AC side of inverter. The main use of power balance theory is to ensure the equilibrium between power generation, power flow, and power consumption within the system. By accurately monitoring and controlling power balance, the theory facilitates efficient utilization of renewable energy, enhances system performance, and mitigates power quality issues. A PI control regulates the actual V_{DC} and V_{DCref} at capacitor terminal, regulating internal bus of UPFC, that is power difference between P_{se} and P_{sh}.

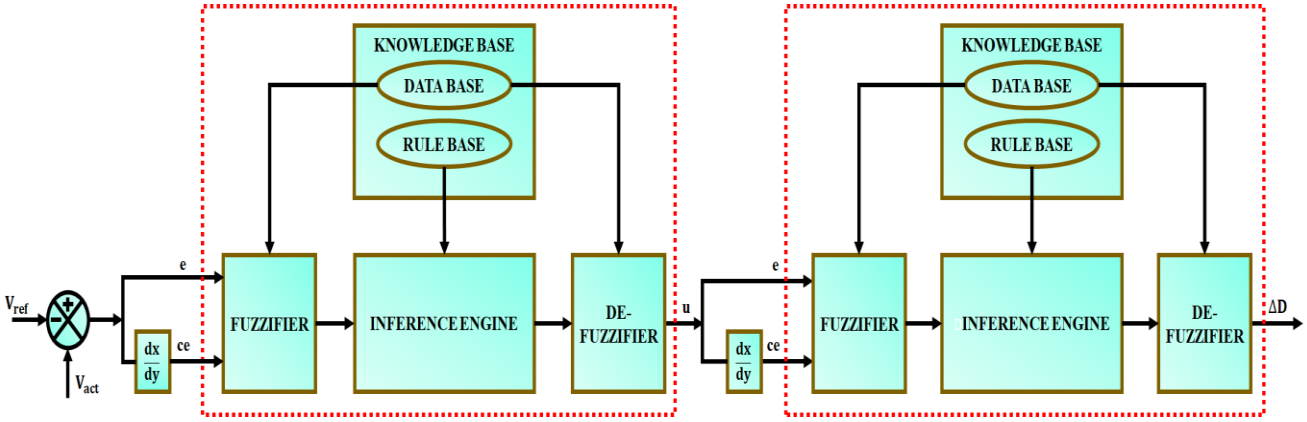

Fig. 5. Structure of CFLS

$$\frac{dV_{DC}}{dt} = -\frac{\omega V_{DC} g_{cap}}{b_{cap}} + \frac{\omega}{b_{cap}}(i_{dsh} - i_{dse}) \qquad (21)$$

As a result, more power is extracted from the source to compensate for power drawn by the load. A line current's d-q components correspond to those of i_{dse} and i_{qse}.

2.5. Cascaded Fuzzy Logic Controller

In general, fuzzy expert systems function mostly based on their rule bases. As an expert system's rule base grows, its execution time also increases. It is possible to develop the enactment of an expert system by reducing its complexity. In this case, a cascade strategy is suggested to lessen the complexity of rule base. The proposed methodology depicts a hierarchical, cascading fuzzy interface of Mamdani type. The use of an appropriate controller, such as CFLC, gives necessary error correction and enhances its dynamic performance. Cascaded control is used to provide overall system control and offers speedy reactions to interruptions. Stabilizing output and consistently ensuring that it is free from fluctuations is the primary objective of the CFLC in UPFC. As already indicated, CFLC's ability to provide quick and precise dynamic reaction attests to its selection as a suitable controller. Two FLCs are a part of CFLC structure, and they are linked in series as shown in Fig. 5. FLC 1 reduces the range of duty ratio for FLC 2.

The FLC mimics the actions of a knowledgeable human operator. It mimics human reasoning to produce a clear answer for issues with incomplete and inaccurate data.

Cascaded fuzzy systems have outputs that become inputs for other systems. A new fuzzy system is created by combining the output of the previous one with the new inputs and inputs of the new fuzzy system. Cascaded evaluations are performed on the entire system. Four variables are considered in this fuzzy system, along with five membership functions. The maximum count of fuzzy rules will be 75, which is equal to FIS1 + FIS2 + FIS3 $(5^2 + 5^2 + 5^2)$.Hence, the entire system may encompass 75 rules, while utilizing the fuzzy cascading technique it just needs$(5^2 + 5^2)$ 50 rules, as seen in Table 1. So, it is discovered that a hierarchical or cascade technique minimizes the size of rule base. Thus, improved control is achieved with effective utilization of CFLC system with reduced rules and quicker response.

Table 1. CFLC Rules

FUZZY RULES		*e*				
		NB	NS	ZE	PS	PB
ce	NB	ZE	ZE	PB	PB	PB
	NS	ZE	ZE	PS	PS	PS
	ZE	PS	ZE	PS	PS	NS
	PS	NS	NS	NS	ZE	ZE
	PB	NB	NB	NB	ZE	ZE

*Zero (ZE), Positive Big (PB), Negative Big (NB), Positive Small (PS) and Negative Small (NS).

2.6. Modelling Of DFIG-WECS

2.6.1. Wind Turbine

The kinetic energy of the wind is transformed into mechanical energy by wind turbines. Its mechanical energy is quantified in terms of the wind's aerodynamic power. The electricity extracted from wind turbine is incapable of being as much as its total capacity because wind speed is unpredictable. The aerodynamic power is described as follows:

$$P = \frac{1}{2}\rho\pi R^2 C_p(\lambda, \beta)\upsilon^3 \qquad (22)$$

From above equation, density of air is specified as ρ, radius of rotor as R, wind speed as υ, co-efficient of power as $C_p(\lambda, \beta)$, depending on shape and geometry of blades of rotor. Also, the pitch angle and speed ratio is characterized as β and λ. Speed ratio at tip is provided as

$$\lambda = \frac{\Omega_t R}{\upsilon} \qquad (23)$$

The wind turbines angular shaft speed is denoted as Ω_t. Similarly, the interrelated function C_p and λ is written as

$$C_p = c_1\left(\frac{c_2}{\lambda} - 1\right)e^{\frac{-c_3}{\lambda}} \quad (24)$$

The positive constants are indicated as c_1, c_2, c_3. The voltage drawn from WECS is made operated at variable speed range with the adoption of suitable generator. Accordingly, this work established DFIG system and the construction is as follows.

2.6.2. DFIG System Design

Due to its tight coupling, asynchronous machines are challenging to model in three phases. The following is a DFIG paradigm in dq-synchronous reference frame.

$$\begin{cases} V_{ds} = R_s I_{ds} + \frac{d}{dt}\varphi_{ds} - \omega_s \varphi_{qs} \\ V_{ds} = R_s I_{qs} + \frac{d}{dt}\varphi_{qs} + \omega_s \varphi_{ds} \\ V_{dr} = R_r I_{ds} + \frac{d}{dt}\varphi_{dr} - (\omega_s - \omega_r)\varphi_{qs} \\ V_{qr} = R_r I_{qs} + \frac{d}{dt}\varphi_{qr} - (\omega_s - \omega_r)\varphi_{ds} \\ where \begin{cases} \varphi_{ds} = L_s I_{ds} + M I_{dr} \\ \varphi_{qs} = L_s I_{qs} + M I_{qr} \\ \varphi_{dr} = L_r I_{dr} + M I_{ds} \\ \varphi_{qr} = L_r I_{qr} + M I_{qs} \end{cases} \end{cases} \quad (25)$$

From Equation (25) stator and rotor current components is specified as I_{ds}, I_{qs} and I_{dr}, I_{qr}, similarly, rotor and stator voltage as V_{dr}, V_{qr} and V_{ds}, V_{qs}, likewise stator and rotor flux is denoted by $\varphi_{ds}, \varphi_{qs}$ and $\varphi_{dr}, \varphi_{qr}$, consequently, stator and rotor resistance is indicated as R_s and R_r. Also, the angular velocity of stator and rotor is represented as ω_s and ω_r and inductance of rotor and stator as L_r and L_s and number of pairs of poles as p.

The following factors determine the dynamics of rotating generator portions:

$$J\frac{d}{dt}\Omega_r = T_{em} - T_L - f_r\Omega_r \quad (26)$$

Here, the electromagnetic and load torque is indicated by T_{em}, T_L, inertia as J, and co-efficienct of viscous friction as f_r. The expression for electromagnetic torque is expressed as

$$T_{em} = p\frac{MV_s}{\omega_s L_s}(\varphi_{qs} I_{dr} - \varphi_{ds} I_{qr}) \quad (27)$$

Establishing the reference frame with stator flux's d-axis, the above equation gets simplified and becomes

$$T_{em} = -p\frac{MV_s}{\omega_s L_s}\varphi_s I_{qr} \quad (28)$$

Therefore, the rotor current is expressed as follows in relation of stator flux:

$$\frac{d}{dt}I_{dr} = \frac{1}{\sigma L_r}\left(V_{dr} - R_r I_{dr} + s\sigma L_r \omega_s I_{qr} - \frac{M}{L_s}\frac{d}{dt}\varphi_{ds}\right) \quad (29)$$

$$\frac{d}{dt}I_{qr} = \frac{1}{\sigma L_r}\left(V_{qr} - R_r I_{qr} + s\sigma L_r \omega_s I_{dr} - s\omega_s \frac{M}{L_s}\frac{d}{dt}\varphi_{ds}\right) \quad (30)$$

Hence, the suggested DFIG system achieves high performance and self-regulating control of both active and reactive power. The voltage generated is converted into DC utilizing PWM rectifier. To control the rectifier voltage enhanced control approach is necessary, and is described as follows.

2.7. Improved Harris Hawks Optimization Algorithm

The voltage transformed into DC requires stabilization, which is achieved in this work by adopting IHHO. In the proposed work, HHO algorithm is enhanced by introducing improvements to its search mechanism and exploration-exploitation balance. The algorithm incorporates enhanced strategies for the selection of leader hawks, local search operators, and adaptive control parameters. These improvements lead to increased convergence speed, improved exploration of the search space, and enhanced global optimization capabilities. The use of the Improved Harris Hawks Optimized Proportional Integral (IHHO-PI) controller is essential in wind energy systems due to its significance in achieving improved system performance and stability. By leveraging nature-inspired optimization techniques, IHHO-PI controller provides a robust and efficient solution for strengthening the DC voltage of WECS, ensuring reliable operation and improved power quality. The flow diagram of IHHO approach is depicted in Fig. 6. The sections that follow provide a derivation of the governing equations:

2.7.1. Exploration Phase

The ultimate focus of Harris hawk hunting is to take down its prey, which is typically a rabbit. Hence, hawks search for rabbit in the beginning. There are two ways to express the exploring procedure. According to the first, hawks' positions ought to be close to their families and their prey. The second method, however, relies on hawks being spread out among different trees. These methodologies' mathematical applicability is represented by the following model:

$$X(t+1) = \begin{cases} X_{rand}(t) - r_1|X_{rand}(t) - 2r_2 X(t)| & q \geq 0.5 \\ (X_{rab}(t) - X_m(t)) - r_3(LB + r_4(UB - LB)) & q < 0.5 \end{cases} \quad (31)$$

Here, iteration at present is specified as t, hawk's position at iteration t and $t+1$ is expressed as $X(t)$ and $X(t+1)$, location of rabbit as $X_{rab}(t)$, and position of hawks selected at random is represented as $X_{rand}(t)$. The parameters r_1 to r_4 be numbers at random ranging within $[0,1]$, UB and LB are the upper and lower search limits. Using random variable q the exploration techniques

are switched between $[0,1]$. The location of hawks mean position is specified as

$$X_m(t) = \frac{1}{n}\sum_{i=1}^{n} X_i(t) \quad (32)$$

From equation above, hawk at position i is specified as $X_i(t)$, and number of hawks in total as n.

2.7.2. Exploitation vs. Exploration

In the HHO, it is possible to change between exploration and exploitation by making use of the escaping energy of the rabbit E during the chasing process. This can be further expressed as follows:

$$E = 2E_0\left(1 - \frac{t}{T}\right) \quad (33)$$

Initial energy of rabbit at random between $[-1,1]$ is denoted as E_0 and maximum iteration as T. When $E \geq 1$ specifies the escaping chance for rabbit, and thus exploration phase is continued by Hawks. Similarly, when $E < 1$, weakness of rabbit is predicted and hawks begin to exploit the position of rabbit.

2.7.3. Exploitation Phase

The exploitation phase of HHO is based on r, that is the chance that rabbit will escape, and E is the escaping energy. The rabbit can successfully escape when $r < 0.5$ and unsuccessfully escape when $r \geq 0.5$. Using the escaping energy, hawks rely on a soft besiege if $|E| \geq 0.5$ hard besiege if $|E| < 0.5$ as appropriate. As a result, it is possible to mathematically model the exploitation process of the HHO based on four chases that take place within besieges.

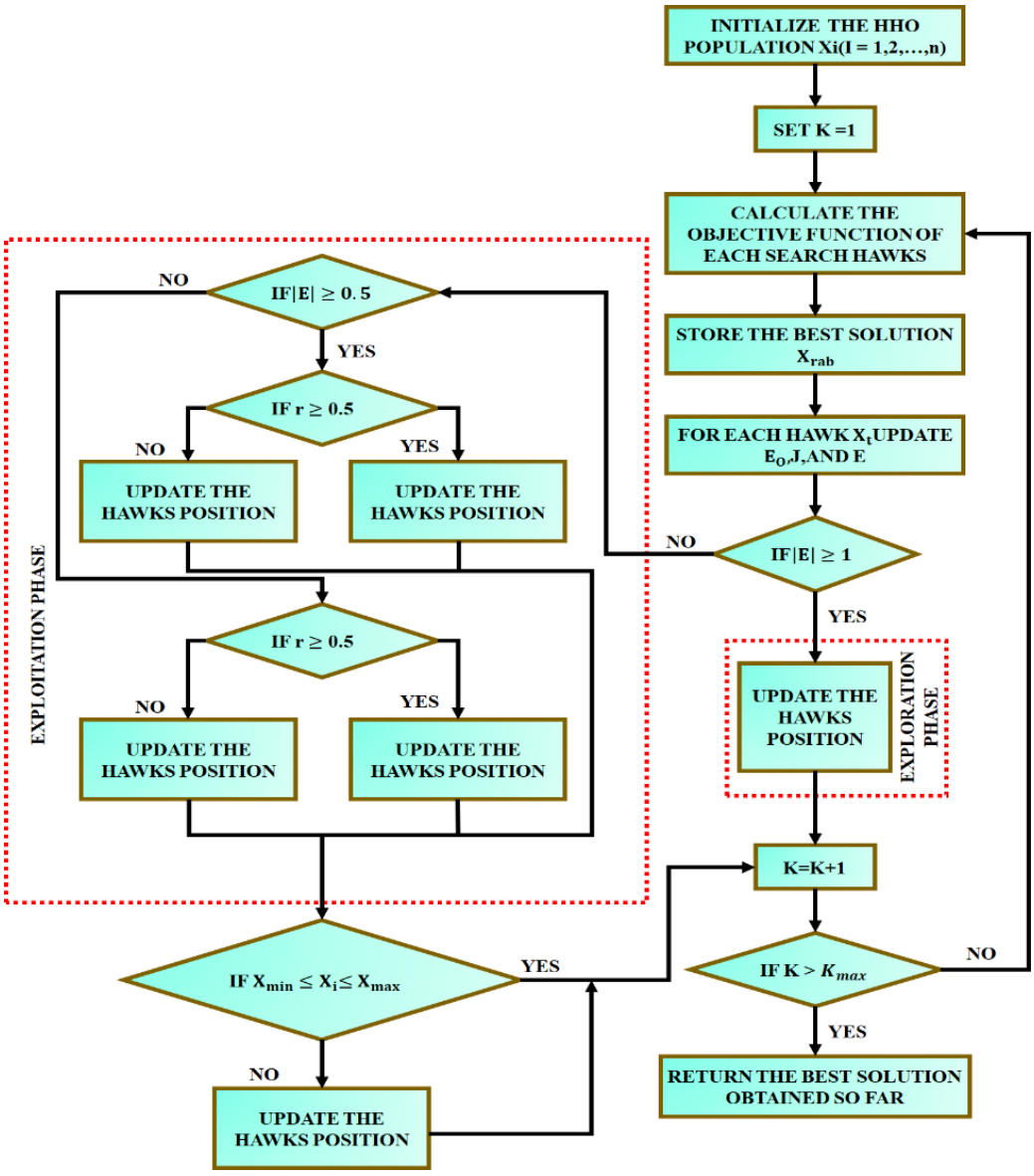

Fig. 6. Flow Chart Representation of IHHO.

2.7.4. Soft Besiege

It appears that the rabbit tries to escape with the assistance of random jumps despite the hawks surrounding it softly when $r \geq 0.5$ and $|E| \geq 0.5$. This is mathematically formulated as follows:

$$X(t+1) = \Delta X(t) - E|JX_{rab}(t) - X(t)| \quad (34)$$

$$J = 2(1 - r_5) \quad (35)$$

$$\Delta X(t) = X_{rab}(t) - X(t) \quad (36)$$

From the expressions above random jumps of rabbit to escape is specified as J and distance between rabbits position as $\Delta X(t)$.

2.7.5. Hard Besiege

It is possible for the hard besiege to occur when $r \geq 0.5$ and $|E| < 0.5$. The hawks have barely surrounded the rabbit in that case. In this case, the action would be as follows:

$$X(t+1) = X_{rab}(t) - E|\Delta X(t)| \quad (37)$$

2.7.6. Progressive Rapid Dives in Soft Besiege

In this besiege, Intelligence differentiated HHO from other swarm methods with respect to the HHO's intelligence strategy. The rabbit is able to run away when $r < 0.5$ and$|E| \geq 0.5$, and the hawks surround it softly. Based on the Levy flight (LF) concept, the following besiege has been formulated:

$$Y = X_{rab}(t) - E|JX_{rab}(t) - X(t)| \quad (38)$$

According to LF, hawks dive is written as

$$Z = Y + S \times LF(D) \quad (39)$$

The dimension problem is specified as D, and vector of random values having size $1 \times D$ is denoted as S. The LF is given by,

$$LF(x) = 0.01 \times \frac{\mu \times \sigma}{|v|^{\frac{1}{\beta}}} \quad (40)$$

$$\sigma = \left(\frac{\Gamma(1+\beta) \times sin\left(\frac{\pi\beta}{2}\right)}{\Gamma\left(\frac{1+\beta}{2}\right) \times \beta \times 2^{\left(\frac{\beta-1}{2}\right)}} \right)^{\frac{1}{\beta}} \quad (41)$$

From the above equation, a constant value of 1.5 is assigned to β, and random values between [0,1] are used for μ and v. Therefore, the position of hawks at preceding iteration is portrayed as

$$X(t+1) = \begin{cases} Y, & F(Y) < F(X(t)) \\ Z & F(Z) < F(X(t)) \end{cases} \quad (42)$$

2.7.7. Rapid Dives with Hard Besiege

The rabbit is exhaustion and is surrounded hardly by the hawks at r = 0.5, |E| = 0.5 in this case. As in Equation (38) to (41), LF is employed to state this besiege, but Y is estimated as follows:

$$Y = X_{rab}(t) - E|JX_{rab}(t) - X_m(t)| \quad (43)$$

2.7.8. Improved HHO Algorithm

The HHO method uses the following expression to send hawks back if their position exceeds the limits:

$$X(t+1) = \begin{cases} X(t+1), & X_{min} \leq X(t+1) \leq X_{max} \\ X_{min} & X(t+1) < X_{min} \\ X_{max} & X(t+1) > X_{max} \end{cases} \quad (44)$$

Here minimal and maximal optimization issue variables are represented as X_{min} and X_{max}. Moreover, to enhance HHO, it is proposed that in case of hawks surpasses, it should return back to rabbit position X_{rab}, which is assumed as optimal solution and the expression is determined by,

$$(t+1) = \begin{cases} X(t+1), & X_{min} \leq X(t+1) \leq X_{max} \\ X_{rab}(t) & X(t+1) < X_{min} \\ X_{rab}(t) & X(t+1) > X_{max} \end{cases} \quad (45)$$

Thus, by utilizing improved strategy enhanced voltage stabilization is achieved thereby resulting in enhanced system performance. To assess the efficacy of the proposed work, a MATLAB examination is performed. Following is a description of the results obtained.

3. RESULTS AND DISCUSSION

The UPFC is tested utilizing the MATLAB/Simulink platform demonstrating improving voltage instability, swell, and transients. Moreover, the system's THD state is also shown. Table 2 discusses the parameters used in MATLAB/Simulink environment.

Case 1: Step Magnitude -0.2

UPFCs that operate with WECS feed are tested to evaluate their effectiveness both under voltage sag conditions and when voltage swell occurs. The first case evaluates the feasibility and suitability of WECS fed UPFC, with a step magnitude value of -0.2 when it encounters voltage sag and the waveforms for concerned voltage sag are shown in Fig. 7 and 8. Accordingly, a 400V source results in 0.2 p.u voltage between 0.1s and 0.2s. In a voltage sag scenario, the input current increases to 50A. To get a clear picture of source voltage and current waveform, case 1 also takes into account a single phase of the source voltage and current. After analyzing load voltage and load current waveforms, it is determined that the proposed WECS-based UPFC design can effectively compensate for voltage sag. Additionally, accurate voltage sag compensation maintains unity power factor. Moreover, real and reactive power waveform is also depicted in Fig. 9, where reactive power is minimized effectively by the adoption of proposed approach.

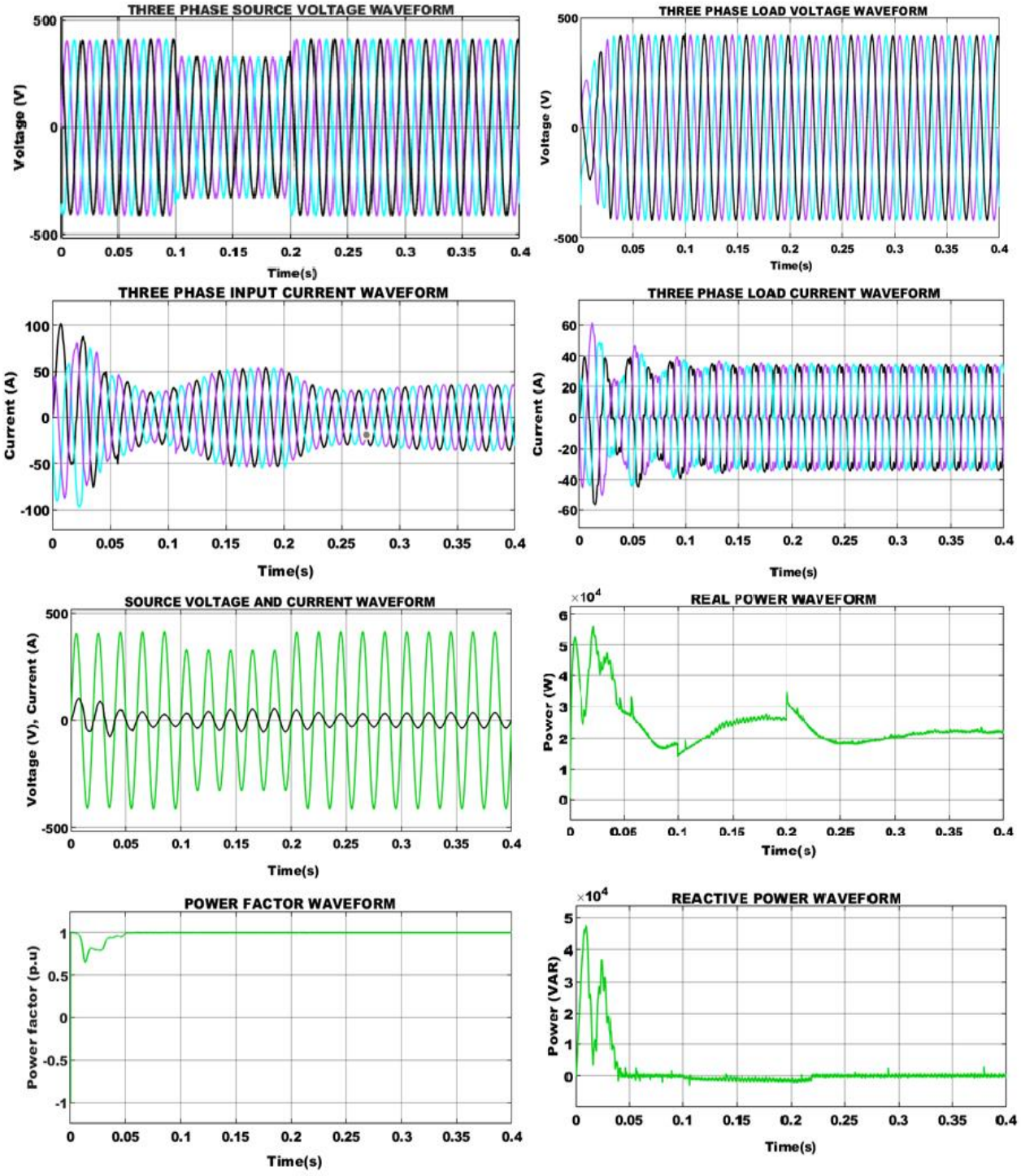

Fig. 7. Simulated output with step magnitude -0.2.

Table 2. Parameter Specification

Parameter	Specification
Load Inductance	10mH
Load Resistance	100Ω
Source Voltage	$330 - 480V$
Source Current	$0 - 30A$

According to Fig. 8, the CFLC assisted DQ theory is utilized for generating reference current signal for the shunt compensator. Additionally, Fig. 8 displays the reference voltage generated using DQ theory for the series compensator signal. The Fig. 8 also displays the actual current waveform of the shunt compensator as well as the voltage waveform of the series compensator. Consequently, WECS-UPFC compensates both the quality of current and voltage in system.

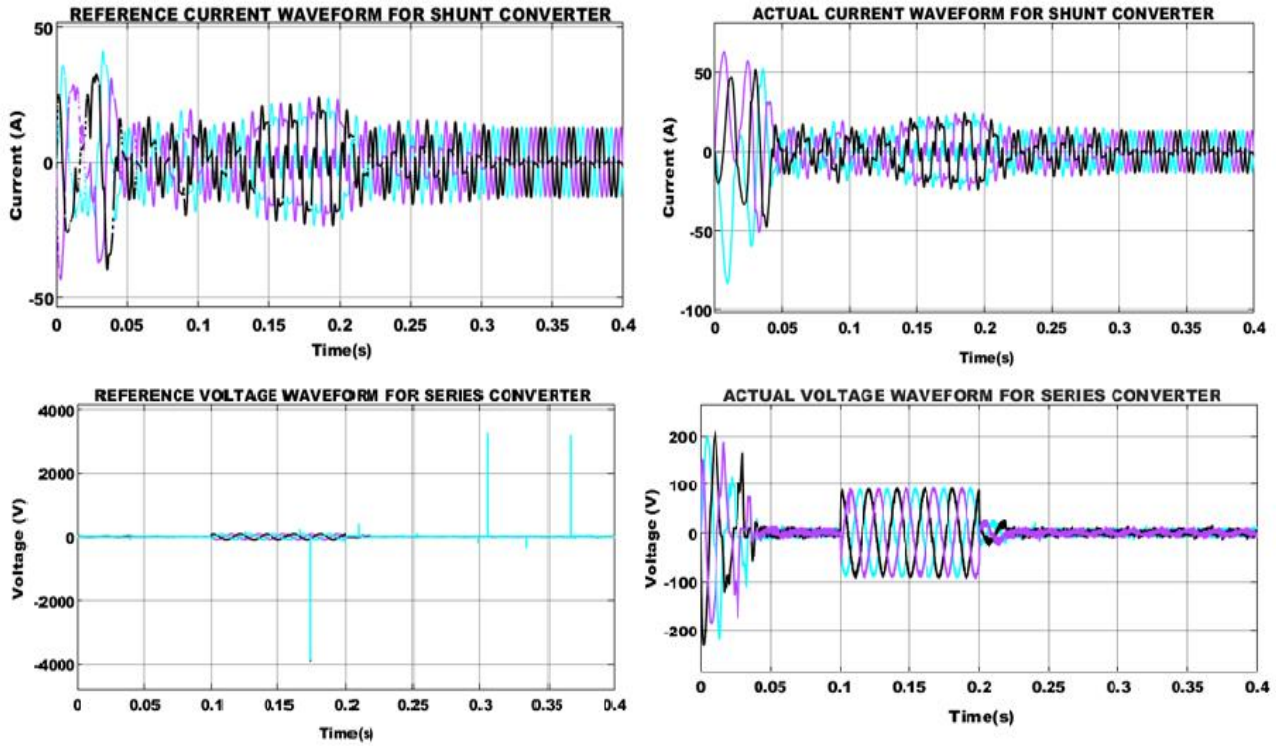

Fig. 8. Voltage sag waveform of series and shunt compensator.

Case 2: Step Magnitude +0.2

Case 2 evaluates WECS-dynamic UPFC's operation in a voltage swell scenario, and relevant waveforms are shown in Fig. 9. In scenario 2, source voltage waveform exhibits a voltage surge of magnitude +0.2 p.u. throughout a time range of 0.1 to 0.2s. The following waveform demonstrates the associated input current waveform, whose magnitude decreases in response to voltage swell. The waveforms for a single phase source voltage and current under voltage swell circumstance are also taken into consideration. Similar to case 1, case 2 likewise achieves a unity power factor. The outstanding compensating performance of series and shunt compensators of suggested UPFC allows for the maintenance of a constant and predictable voltage and current on load side.

The UPFC's series and shunt compensators generate the necessary compensation current and voltage signals to lessen the effects of voltage swell conditions. DQ theory is employed to generate reference voltage for series compensator, while CFLC-assisted DQ theory is utilized to provide the reference current signal for shunt compensator. A harmonics-free reference current signal is generated via CFLC assisted dq theory, as seen in Fig. 10. Voltage sag issue is lessened by Series compensator, which injects a voltage of magnitude 70V.

The output voltage obtained using DFIG is demonstrated in Fig. 11 (a) along with PWM rectified output in Fig. 11(b). it is noted that, the DFIG output is not stable, owing to variations in wind speed at initial stage. After 0.15 seconds, a distortion-free stable voltage of 600V is attained. Similarly, a stable voltage of 600V is maintained with only slight variations at the rectifier output's first stage according to the proposed IHHO algorithm. Hence stabilized voltage of 600V is sustained constant.

THD is a critical metric for assessing the degree of harmonic distortion in voltage or current waveforms. The THD outcomes obtained in the proposed is depicted in Fig. 12. An improved THD value of 2.12% is noted, fulfilling the specifications of the IEEE standard.

The comparison of controllers like PI, FLC and CFLC for UPFC system in terms of THD is illustrated in Fig. 13. The proposed CFLC system is found to have a THD value of 2.12%, whereas PI and FLC reach 4.3 and 3.21%, respectively. Therefore, it can be said that using CFLC leads to an enhanced THD value of 2.12%, along with less harmonics and best possible system performance.

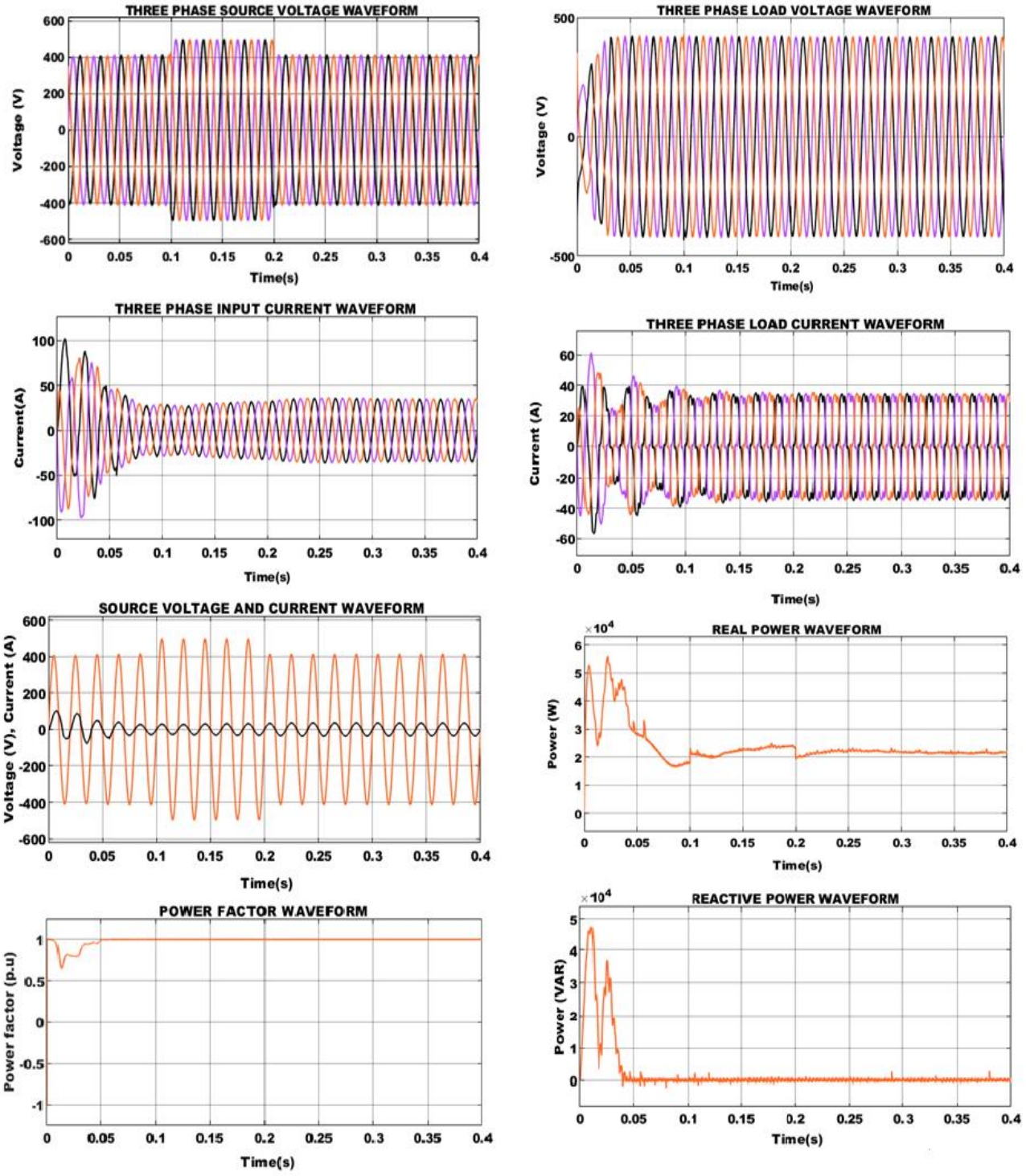

Fig. 9. Simulated Voltage Swell Waveforms with Step Magnitude +0.2.

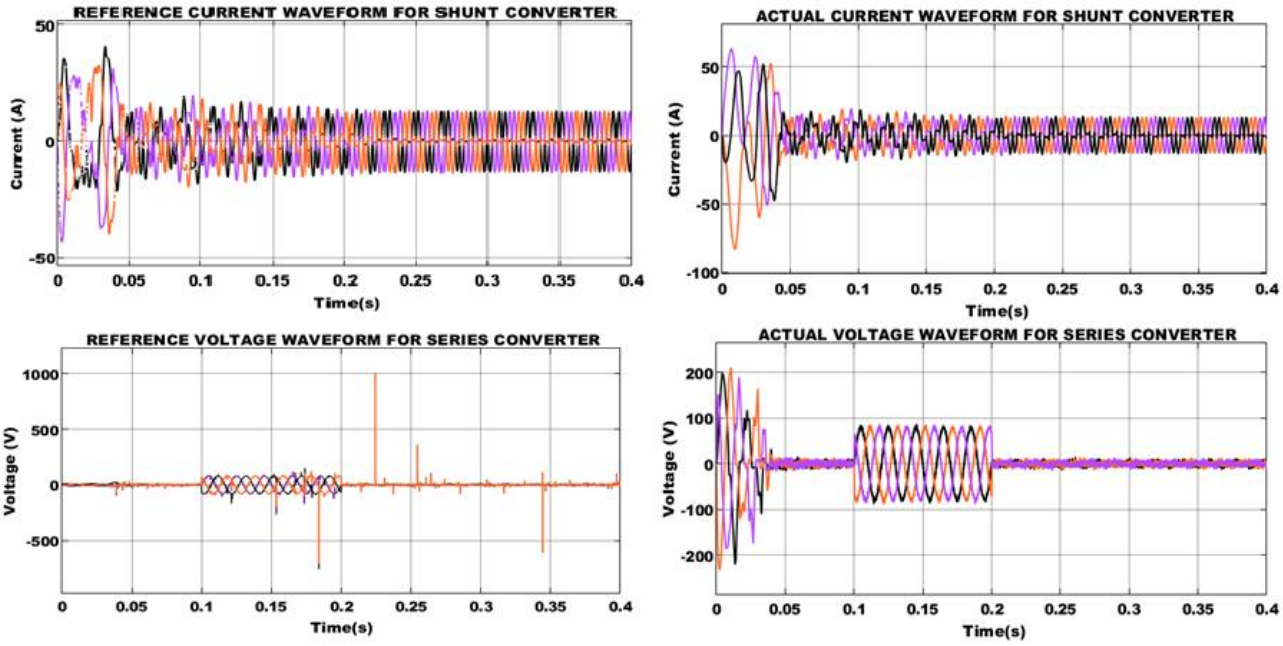

Fig. 10. Voltage Swell Waveforms for Series and Shunt Compensator.

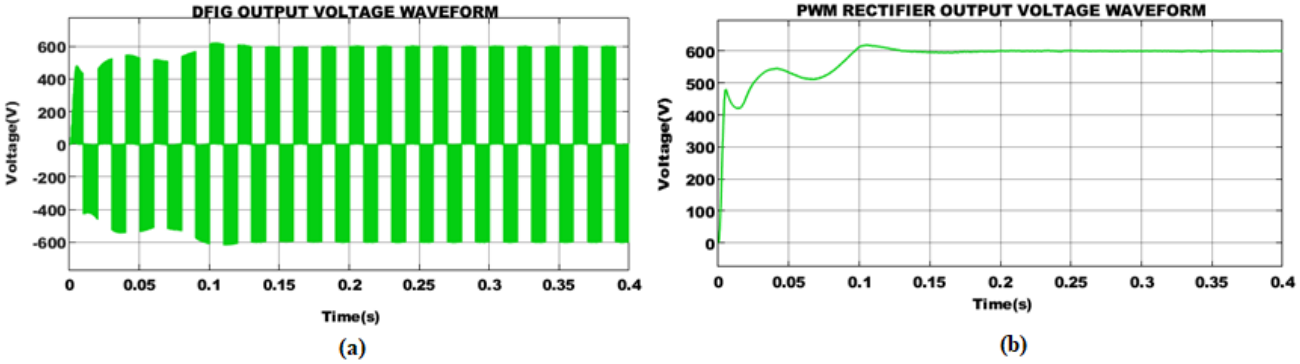

Fig. 11. (a) DFIG Output (b) PWM Rectifier Output.

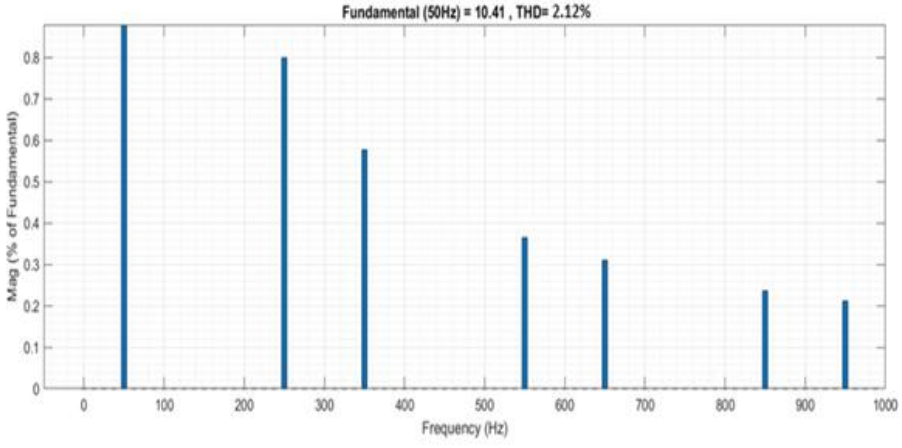

Fig. 12. THD Waveform.

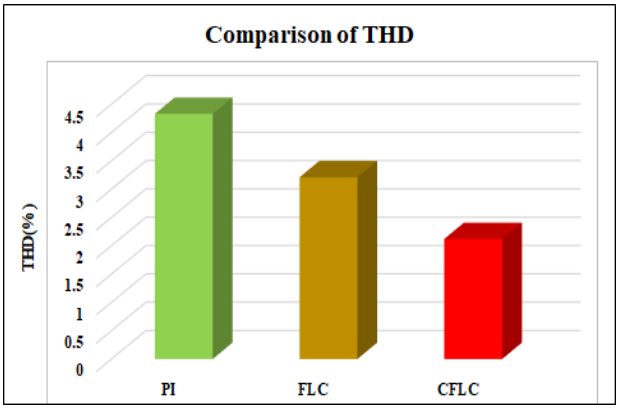

Fig. 13. Comparison of THD.

4. CONCLUSION

The growing use of solid-state controls for power conversion has created a significant issue for power quality. Due to widespread use of goods based on power electronics, it is currently difficult to fulfil high PQ standards. This paper provides effective control scheme for UPFC relying on CFLC to address problems with power quality in transmission networks. The adoption of IHHO results in stabilized voltage from PWM rectifier. Based on the suggested CFLC technique, the compensating efficacy of voltage sags increased. It is established in MATLAB that the modelling for proposed WECS fed UPFC with wise control techniques is capable of resolving voltage instability and voltage swell conditions. The effectiveness of proposed UPFC system is demonstrated by displaying the load voltage profiles in situations of voltage instability, voltage transient, harmonic, and voltage flicker for UPFC system. Consequently, the proposed strategy is beneficial in maintaining PQ and power factor at unity. Furthermore, an improved THD value of 2.12% is achieved which is comparatively low, thereby which recognizes the significance of suggested PQ development strategy.

REFERENCES

[1] Abbas, S.R.; Kazmi, S.A.A.; Naqvi, M.; Javed, A.; Naqvi, S.R.; Ullah, K.; Khan, T.U.R.; and Shin, D.R. 2020. Impact analysis of large-scale wind farms integration in weak transmission grid from technical perspectives. Energies 13(20): 5513.

[2] Khandelwal, P.; and Modi, B. 2015. Modeling, simulation of UPFC and its effect on power system protection. International Journal of Emerging Research in Management &Technology 4(5): 138-147.

[3] Kavin, K.S.; and Subha Karuvelam, P. 2023. PV-based grid interactive PMBLDC electric vehicle with high gain interleaved DC-DC SEPIC Converter. IETE Journal of Research 69(7): 4791-4805.

[4] Mohanty, A.; Viswavandya, M.; Ray, P.K.; and Patra, S. 2014. Stability analysis and reactive power compensation issue in a microgrid with a DFIG based WECS. International Journal of Electrical Power & Energy Systems 62: 753-762.

[5] Nagaraju, G.; and Shankar, S. 2020. Power quality improvement of wind energy conversion system with unified power quality controller: A hybrid control model. Transactions of the Institute of Measurement and Control 42(11): 1997-2010.

[6] Mosaad, M.I.; Abu-Siada, A.; Ismaiel, M.M.; Albalawi, H.; and Fahmy, A. 2021. Enhancing the fault ride-through capability of a DFIG-WECS using a high-temperature superconducting coil. Energies 14(19): 6319.

[7] Mohanty, A.; Patra, S.; and Ray, P.K. 2016. Robust fuzzy-sliding mode based UPFC controller for transient stability analysis in autonomous wind-diesel-PV hybrid system. IET Generation, Transmission & Distribution 10(5): 1248-1257.

[8] Bharti, O.P.; Verma, A.; Saket, R.K.; and Nagar, S.K. 2021. DFIG Based WT for Frequency Control along with AGC in Multi-Area Systems. GMSARN International Journal 15: 317-330.

[9] Goud, B.S.; Reddy, C.R.; Bajaj, M.; Elattar, E.E.; and Kamel, S. 2021. Power Quality Improvement Using Distributed Power Flow Controller with BWO-Based FOPID Controller. Sustainability 13(20): 11194.

[10] Sankarganesh, R.; and Kumar, P.A. 2019. Mitigation of Harmonics and Power Quality Improvement for Grid-Connected Wind Energy System using Unified Power Flow Controller Based on Spontaneous Energy Optimization Algorithm. International Journal of Engineering Inventions 8(1): 92-101.

[11] Sarita, K.; Kumar, S.; Vardhan, A.S.S.; Elavarasan, R.M.; Saket, R.K.; Shafiullah, G.M.; and Hossain, E. 2020. Power enhancement with grid stabilization of renewable energy-based generation system using UPQC-FLC-EVA technique. IEEE Access 8: 207443-207464.

[12] Adetokun, B.B.; and Muriithi, C.M. 2021. Application and control of flexible alternating current transmission system devices for voltage stability enhancement of renewable-integrated power grid: A comprehensive review. Heliyon 7(3): e06461.

[13] Mbae, M.; and Nwulu, N. 2022. Impact of hybrid FACTS devices on the stability of the Kenyan power system. International Journal of Electrical and Computer Engineering (IJECE) 12(1): 12-21.

[14] Ghaedi, S.; Abazari, S.; and Arab Markadeh, G. 2022. Novel non-linear control of DFIG and UPFC for transient stability increment of power system. IET Generation, Transmission & Distribution 16(19): 3799-3813.

[15] Shahdadi, A.; ZM-Shahrekohne, B.; and Barakati, S.M. 2019. Analyzing Impacts of FACTS devices in dealing with short-term and long-term wind turbine faults. Journal of Operation and Automation in Power Engineering 7(2): 206-215.

[16] Le Minh Thang, D.T.H.; Le-Duc, T.; and Khanh, B.Q. 2023. GA Based Multi-Objective Optimizing Size and Location of One D-STATCOM for Global Voltage Sag Mitigation in Distribution System. GMSARN International Journal 17: 1-7.

[17] Muisyo, I.N.; Muriithi, C.M.; and Kamau, S.I. 2022. Enhancing low voltage ride through capability of grid connected DFIG based WECS using WCA-PSO tuned STATCOM controller. Heliyon 8(8): e09999.

[18] Mosaad, M.I. 2020. Whale optimization algorithms-based PI controllers of STATCOM for renewable hybrid power

system. World Journal of Modelling and Simulation 16(1): 26-40.

[19] Prasad, D.D., Chandini, B.L., Mahesh, S., Naveen, S.S.; and Babu, S.M. 2021. Power Quality Improvement in WECS Using ANN—Statcom. International Journal for Modern Trends in Science and Technology 7: 160-165.

[20] Habib, S.; Abbas, G.; Jumani, T.A.; Bhutto, A.A.; Mirsaeidi, S.; and Ahmed, E.M. 2022. Improved whale optimization algorithm for transient response, robustness, and stability enhancement of an automatic voltage regulator system. Energies 15(14): 5037.

[21] Sule, A.H.; Mokhtar, A.S.; Jamian, J.J.B.; Khidrani, A.; and Larik, R.M. 2020. Optimal tuning of proportional integral controller for fixed-speed wind turbine using grey wolf optimizer. International Journal of Electrical and Computer Engineering (IJECE) 10(5): 5251-5261.

[22] Lotfi, C.; Youcef, Z.; Marwa, A.; Schulte, H.; El-Arkam, M.; and Riad, B. 2023. Optimization of a Speed Controller of a WECS with Metaheuristic Algorithms. Engineering Proceedings 29(1): 7.

[23] Shehata, A.A.; Refaat, A.; Ahmed, M.K.; and Korovkin, N.V. 2021. Optimal placement and sizing of FACTS devices based on Autonomous Groups Particle Swarm Optimization technique. Archives of Electrical Engineering 70(1): 161-172.

[24] Pandya, M.; and Jamnani, J.G. 2019. Transient stability assessment by coordinated control of SVC and TCSC with particle swarm optimization. Int. J. Eng. Adv. Technol 9(1): 2506-2510.

[25] Alsammak, A.N.; and Mohammed, H.A. 2021. Power quality improvement using fuzzy logic controller based unified power flow controller (UPFC). Indonesian Journal of Electrical Engineering and Computer Science 21(1): 1-9.

[26] Sarita, K.; Kumar, S.; Vardhan, A.S.S.; Elavarasan, R.M.; Saket, R.K.; Shafiullah, G.M.; and Hossain, E. 2020. Power enhancement with grid stabilization of renewable energy-based generation system using UPQC-FLC-EVA technique. IEEE Access 8: 207443-207464.

[27] Tarik, R.; and Adil, B. 2022. Wind farm connected to a grid using fuzzy logic controller based the unified power flow controller. International Journal of Power Electronics and Drive Systems 13(3): 1802.